Chemical Engineering Journal 461 (2023) 141964

Contents lists available at ScienceDirect

Chemical Engineering Journal

journal homepage: www.elsevier.com/locate/cej

Interplay of regio-selectively modified dendritic silica particles with styrene-butadiene rubber: The route towards better tires with lower rolling-resistance and higher grip

Enzo Moretto [a,c], Charlotte Stoffels [a], Carlos Eloy Federico [a], Vincent Rogé [a], Mariapaola Staropoli [a], Iikpoemugh Elo Imiete [a], Jean-Nicolas Audinot [a], Pascal Steiner [b], Benoît Duez [b], Damien Lenoble [a], Jean-Sébastien Thomann [a,*]

[a] Materials Research and Technology Department, Luxembourg Institute of Science and Technology, 41 Rue du Brill, L-4422 Belvaux, Luxembourg
[b] Goodyear S.A, Avenue Gordon Smith, L-7750 Colmar-Berg, Luxembourg
[c] Department of Physics and Materials Science, University of Luxembourg, L-4365 Esch-sur-Alzette, Luxembourg

ARTICLE INFO

Keywords:
Mesoporous silica
Silica-rubber composite
Silanization
Regio-selective silanization
SIMS
Elemental mapping

ABSTRACT

The current study presents for the very first time to our knowledge the synthesis, characterization, and application of regio-selectively modified dendritic silica particles (RMDS) in tire rubber composites. So far, no study has ever reported mesoporous silica bringing greater mechanical properties than small fractal precipitated silica. With mechanical testing (DMA, tensile strength) and advanced imaging (TEM-EDS, HIM-SIMS, micro-CT), it was demonstrated that dendritic particles enable superior mechanical reinforcement of rubber-based nanocomposites without any drawback as usually reported with fractal fillers. On one side, their modified porous surface mimics the porous aggregates formed by classic fillers, enabling the rubber chains to permeate the pores and closely interact with the particles. On the other side, unlike fractal fillers, RMDS consist of single particles instead of aggregates, and therefore do not suffer as much from the Payne effect and irreversible dislocations under mechanical solicitations. Also, the excellent dispersibility of RMDS allows to combine them with small amount of fractal filler. Dual filler composite shows superior mechanical performances versus materials using one filler family, leading to higher reinforcement, better traction and rolling resistance indicators. The use of porous particles as "unbreakable" fillers for rubber with a small amount of fractal silica as additive fillers paves the way for novel reinforcing dual-filler systems to be used in disruptive tires technology.

1. Introduction

For technical applications, polymers are almost always combined with fillers to drastically improve their performances, as neat polymer properties are often unsatisfactory. For the reinforcement of rubber-based tires, silica has been used for decades and since then many advances in this technology have been made. The first and major one has been the use of organosilanes that enable better dispersion and interaction between the mineral polar hydrophilic material silica and the organic hydrophobic polymer matrix. Today, many different strategies aiming at further rubber reinforcement from fillers have been investigated. Original materials like clays [1], or graphene oxide [2] have been the topic of extensive research and brought new functionality to composite materials. Other strategies focus on the filler morphology and its effect on the composite properties are well investigated [1,3,4]. When it comes to the morphology of silica particles, mesoporous structures are a vast area of research. Since the first filed patent [5] in 1971, and the emergence of MCM-41[6] and SBA-15 structures [7], research in this area has flourished in wide variety of applications as scientists have recognized the potential of these structures. Initially seen as potent molecular sieves, their large specific surface area, the variety of structures, size, and synthesis processes opened the way for a wide range of applications. Mesoporous silica has been reported for drug delivery systems [8,9], contrast enhancing agent carriers in medical imagery [10], water depollution [11], gas separation [12], column chromatography [13], or catalysis [14,15]. More specifically for rubber materials, porous systems have been used to enhance silicon thermal and optical properties [16], or as antioxidant release in styrene-butadiene rubber

* Corresponding author.
E-mail address: jean-sebastien.thomann@list.lu (J.-S. Thomann).

https://doi.org/10.1016/j.cej.2023.141964
Received 14 October 2022; Received in revised form 11 January 2023; Accepted 14 February 2023
Available online 18 February 2023

(SBR) composites [17]. For their mechanical reinforcement, the interest in mesoporous silica is driven by the high surface area that leads to strong interactions between fillers and the polymeric matrix. Indeed, the reinforcing effect of fillers relies on its ability to interact with the polymer and to change the chains dynamic. On top of its ability to bond with the matrix, the percolation and the formation of a filler network use to transmit stresses and to trap rubber in between particles. When it comes to percolation, the particle size and shape play a major role. It has been shown that silica forming fractal-shaped aggregates have a lower percolation threshold than spherical colloidal particles [18]. Indeed, fractal-shaped clusters expose a greater surface area and trap more polymer at lower filler loading. The same reasoning applies to mesoporous silica particles because porosity provides a high surface of interaction due to the permeation of the polymer inside it. One limitation of fractal fillers is the irreversible deformation and reorganization caused by the mechanical solicitation of fractal aggregates, leading to energy dispersive phenomenon known as Payne and Mullins effect [19–21]. The hypothetical expected benefit of porous silica particles over fractal fillers can be described as follows. The porous particles are not subjected to irreversible mechanical deformation, unlike small silica particles aggregates of comparable surface, while still endorsing the role of crosslink nodes and reinforcing agents. This may reduce the rolling resistance behavior of such composites, whilst providing properties such as traction to such tire tread materials. So far, most studies have used the ordered, narrow pore size (2–3 nm) MCM-41 mesoporous silica, with or without surface modification, in combination with natural rubber (NR) [22], styrene-butadiene rubber SBR [23], styrene-butadiene and nitrile-butadiene rubber (SBR-NBR) [24], and ethylene-propylene diene monomer rubber (EPDM) rubber [25], and have shown reinforcement. However, there is no clear perspective about the role played either by the porous structure features or by the chemical modification of the silica surface on the composite properties. Indeed, for pores as small as the one of MCM-41 (2–3 nm channel diameter), no study relates that rubber polymer chains of 10 000 g/mol – 100 000 g/mol permeate inside pores under classic rubber dry mixing conditions and generate reinforcement. Studies achieving the polymer confinement inside mesopores used either high pressures [26], super-critical CO_2 as solvent for the monomer [27], low molecular weight resins [28] or modified silica [29,30] that are infiltrated with monomers upon further vulcanization. The use of larger pore sizes and larger structures [31,32] or in combination with silanization of silica foam [33] has proven to be an efficient way to reinforce epoxy resin. Unfortunately, the cluster size is too large for rubber reinforcement. Another critical physical aspect of the polymer reinforcement with silica is the fillers dispersion and their coupling to the matrix. The usual strategy is to graft organosilanes on particles to increase their hydrophobicity and to enable their bonding to the polymer chains. In our previous work [34], the strategy of a silica pre-treated with two different silane for reinforcing rubber was reported. The mercaptosilane was used as the coupling agent, and the alkylsilane was designed to mitigate the mercaptosilane reactivity and to enhance the silica dispersion. In the present work, we achieved a unique regio-selective silanization of dendritic silica particles featured by large pores size. The mercaptosilane is co-condensed in the frame of the silica during the particle growth, and an alkylsilane is grafted on the periphery of particles by preventing it to access inside the pores with the soft template already in place. A few mesoporous silica with selective dual functionalization have been reported [35,36], and all with pore below 10 nm, which are more convenient to control and prevent silane migration inside the pores. The full characterization of the newly synthesized regio-selectively modified dendritic particles (RMDS) and its application to tire rubber compounds are reported here. Furthermore, the regio-selective silanization of the porous particles was confirmed via their direct elemental mapping with the help of a Helium Ion beam Microscope (HIM) coupled with a Secondary Ion Mass Spectroscopy (SIMS). After incorporation into an SBR-BR rubber matrix and the characterization of its mechanical properties, this newly synthesized filler was compared to a fractal commercial filler used in an industrial tire tread compounds provided by Goodyear. RMDS provides reinforcement with better fatigue resistance and rolling resistance of tire tread rubber composites. The permeation of polymer into the mesopores and the absence of particles dislocations (unlike the aggregates of fractal fillers) leads to a low hysteresis and a reduced Payne effect. Only a very low number of cavities are detected by computed micro-tomography after cycling the RMDS compounds with tensile fatigue testing. However, the excellent dispersibility of the filler, its size, and its spherical shape prevent sufficient rubber reinforcement to reach the performance level of HDS 200MP. Thus, adding a small amount of fractal fillers, fills the gaps between RMDS particles and increases the filler-filler interaction. This new dual-filler system leads to significantly improved properties of rubber-based nanocomposites in terms of reinforcement, fatigue resistance, wet traction and rolling resistance indicators.

2. Experimental section

The list of chemicals used in the experimental section and the description of the equipment and measurements methodologies used for the synthesis and characterization of silica particles and silica-rubber composites are available in the **experimental section of the Supporting Information.**

2.1. Synthesis of regio-selectively modified dendritic silica particles

The synthesis of regio-selectively modified dendritic silica particles is derived from the synthesis of stellate mesoporous silica particles previously reported [37]. In an Orb Pilot 50 L reaction vessel, 34.7 g of triethanolamine and 192.0 g of hexadecyltrimethylammonium p-toluene sulfonate are dissolved in 10.0 L of de-ionized water. The solution is heated at 80 °C and mixed for 120 min. Then, 1458.0 g of tetraethoxysilane (TEOS) are added. The reaction starts and is kept at 80 °C under stirring until the end of the process. 15 min after the addition of TEOS, 166.3 g of 3-mercaptopropyltriethoxysilane (MPTES) are added to the reaction vessel. 120 min after the addition of TEOS, 167.3 g of hexyltrimethoxysilane (C6) are added. The reaction is then carried out for another 120 min at 80 °C under stirring. At the end of the reaction, stirring is stopped and the silica particles are let to settle at the bottom of the reaction vessel. The supernatant above the settled silica is removed from the vessel via a pump and 15 L of de-ionized water are added. Silica and water are mixed for 12 h at room temperature, stirring is stopped and the silica particles are let to settle at the bottom of the reaction vessel. Again, the supernatant is removed, and 15 L of ethanol are added. Silica and ethanol are mixed for 12 h. at reflux temperature under stirring. Finally, stirring is stopped and silica particles are let to settle at the bottom of the reaction vessel. The ethanol supernatant is removed. The highly concentrated silica particles in ethanol are then separated by centrifugation (4700 g for 1 h). Regio-selectively functionalized stellate silica is then dried in an oven at 110 °C for 48 h and stored in a sealed container. Additionally, Stöber particles, non-modified stellate mesoporous silica particles and bromine-labelled regio-selectively modified dendritic silica particles have been synthesized. Their respective synthesis protocol is available in **Supporting Information**. Stöber particles consist in spherical and non-porous colloidal silica of a controlled size (here with a diameter of 110 nm). Together with non-modified stellate mesoporous silica, these particles have been used to assess the impact of morphology and silanization onto the rubber composite properties. Bromine-labelled regio-selectively modified dendritic silica particles have been synthesized for imaging purposes.

2.2. Silica-rubber composites fabrication

Silica particles were incorporated in a SBR-BR rubber matrix for the fabrication of silica-rubber composites. The ingredients and recipe for the fabrication of silica-rubber composites can be found in **Table S1 of**

the Supporting Information. The silica composition of the composites is summarized in **Table S2 of the Supporting Information**.

3. Results and discussions

3.1. Synthesis and characterization of regio-selectively modified dendritic silica (RMDS)

The dendritic silica particles were synthesized via a surfactant soft-templating sol–gel method. During such a process, the silica precursor, usually TEOS, polymerizes via hydrolysis-condensation to form the silica particles. The soft template surfactant is forming micelles whose shape and size are dictated by concentration and temperature conditions. The inter-molecular interactions between the surfactant and silica oligomers allow for the silica frame to grow around the surfactant micelle. This phenomenon causes the growth of the dendritic porous silica. Advantage was taken of this process to purposely graft silanes at specific location. First, the mercaptosilane MPTES was co-condensed with TEOS during the growth of the particles. This approach ensures its uniform distribution on the silica frame. At this stage, the pores of particles are still filled with the surfactant. Taking advantage of these circumstances, grafting of the alkylsilane is the next logical step to ensure this silane is mainly connected to the periphery of silica particles. After synthesizing the silica particles, the surfactant is removed to reveal the pores. Fig. 1 below illustrates schematically the synthesis of the regio-selectively modified dendritic silica.

The reaction conditions and the concentration of mercaptosilane were carefully chosen to ensure that the co-condensation of the mercaptosilane did not affect the size nor the structure of particles. Indeed, it has been reported that the use of organosilane may disturb the inter-molecular interactions of surfactant molecules or the silica-micelles interaction. This has been described by Möller et al. for the synthesis of fiber-like mesoporous silica [38]. The step of alkylsilane grafting is carried out as a simple post-growth modification of the particles. The newly synthesized regio-selectively modified dendritic silica particle were fully characterized and results are shown in **Figure S1 of the Supporting Information**.

Transmission Electron Microscope (TEM) images in Fig. S1a. and b. show that the dendritic porous structure is retained despite the introduction of MPTES in the silica matrix. TGA curves display the mass-losses associated with volatiles desorption (below 100 °C), surfactant traces desorption and pyrolysis at 240 °C and silane pyrolysis at around 500 °C-550 °C. It has been reported that alkyl chains are more stable at a higher temperature than mercapto moieties, hence different pyrolysis temperature are observed [38]. TGA data of un-modified stellate silica and mercapto-functionalized (Stellate-SH) are presented in **Figure S2 of the Supporting Information**. The lack of peak at about 130 °C on the dTGA spectrum of silanized silica particles reveals different dehydroxylation mechanisms when compared to the non-modified mesoporous silica ones. This observation can be explained by the lower amount of silanol left to be de-hydroxylated on modified silica particles after their consumption by silanization. Regio-selectively modified dendritic silica share the same two peaks at respectively 370 °C and 500 °C that are attributed to the pyrolysis of mercapto groups and alkyl chain (propyl and hexyl), respectively. The intensity of the second peak is higher in the case of the regio-selectively silanized silica because of the grafting of hexyltrimethoxysilane, increasing the amount of alkyl chains present within the material. In the case of non-modified stellate silica particles, two peaks can also be observed, even though the first one is centered around a lower temperature than in the case of modified silica. Those two peaks are assigned to the pyrolysis of the residual surfactant. The co-condensation of MPTES in the stellate frame leads to the addition of 3.8 % of mass. The grafting of hexyltrimethoxysilane adds 5.7 % of additional mass. Overall, about 9.5 % of the mass of RMDS particles correspond to the grafted silanes. The sharp drops in mass observed at 750 °C in TGA and dTGA curves of Fig. S1**(c) and S2** result from the gas switch from pure N_2 to N_2/O_2 mixture at 750 °C. It leads to the oxidation of the remaining organic matter. Covalent bonding of silane is confirmed by ^{29}Si solid state NMR in Fig. S1**d.**, with the presence of T groups between −50 ppm and −70 ppm. Nitrogen adsorption porosimetry results are presented in Fig. S1**e. and S1f**. The introduction of mercaptopropyl moieties reduces the pore volume and specific surface area, but not as much as the addition of hexyl chains, which seems to drastically reduce the adsorption of the gas molecules to the mesoporous surface, as proven by the decrease of pore volume from 2.61 cm^{-3}/g to 1.54 cm^{-3}/g. The pore size distribution was calculated from the nitrogen adsorption data using the DFT model [39]**.** It shows wide open pores with a diameter of about 28 nm, close from sizes observed by SEM (see **Figure S12, 19** nm ± 6 nm). XRD characterization of RMDS material was not carried as it does not display an organized "crystalline-like" structure.

3.2. Dendritic silica regio-selective modification characterization

The regio-selective grafting of the mercaptosilane within the silica frame and the alkylsilane on the out-skirt of the particles has been characterized by Scanning Transmission Electron Microscopy coupled to an Energy Dispersive X-rays Spectroscope (STEM-EDS) and Helium Ion Microscope coupled with a Secondary Ion Mass Spectrometer (HIM-SIMS). STEM-EDS micrographs and as well as Scanning Electron Microscopy (SEM) images are shown in Fig. 2**.** Image (b) shows sulphur atoms in green. Compared to the particles structure depicted in (a), it can be confirmed that sulfur is distributed evenly across the silica particles and no segregation can be observed from these images. SEM images (c) et (d) offer another perspective on the silica particle size distribution and porous structure.

To investigate the consequences of the two-steps silanization process of dendritic silica and the spatial distribution of the alkylsilane on the porous silica particles, an alternative regio-selectively modified dendritic silica was synthesized by substituting the hexyltrimethoxysilane by 7-bromoheptyltrimethoxysilane (see synthesis protocol in

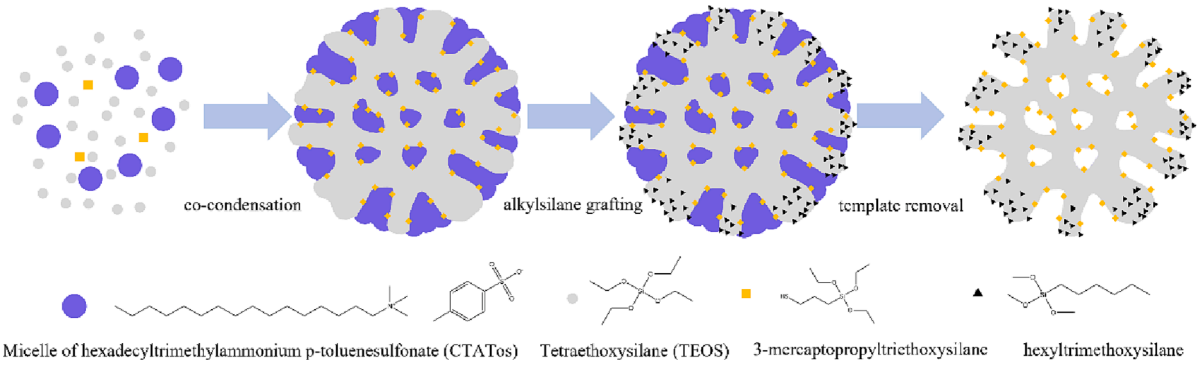

Fig. 1. Schematic view of the regio-selectively modified dendritic silica particles (RMDS).

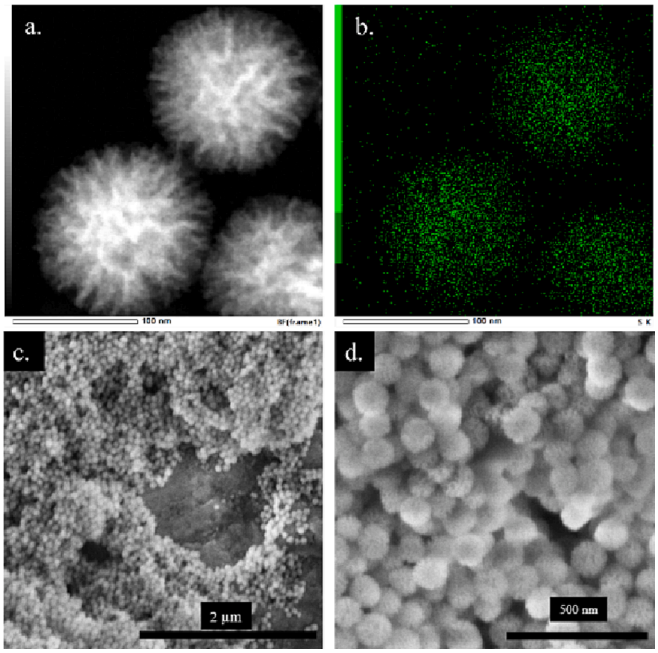

Fig. 2. STEM bright field (BF) images of regio-selectively modified dendritic silica particles (a) and EDS micrographs of sulphur (b), and SEM images (c,d).

Supporting Information). This silane was chosen for its similar size and structure, to mimic as much as possible the original hexyltrimethoxysilane. The bromine atom is used as a labelling agent as carbon alone would not enable to discriminate mercapto- from alkylsilane since both contain carbon atoms.

The distribution of bromine across the silica was mapped by elemental mapping of the particles by nano-Secondary Ion Mass Spectroscopy (SIMS) using a Helium Ion Microscope coupled with a SIMS detector. Fig. 3 display oxygen (^{16}O), carbon (^{12}C–^{12}C), and bromine (^{79}Br) distribution. Larger field of view images are shown in **Figure S3 of Supporting Information**.

Oxygen mapping allows to clearly distinguish the silica particles. The distribution of carbon across the particles is homogeneous and in agreement with the TEM-EDS images. This is to be expected due to the co-condensation of the mercaptopropyl silane during the particle's growth. Despite the low concentration of bromide per molecule, and by voxel sputtered, the SIMS mapping shows the decrease of bromine density inside particles. Especially for isolated particles, a distinctive crown of bromine can be seen. Similar materials architecture have been characterized by Z-contrast STEM, [35]or by porosimetry and fluorescence labelling of reactive moieties [36]. This is the first direct imaging characterization ever reported for multifunctional porous silica particles.

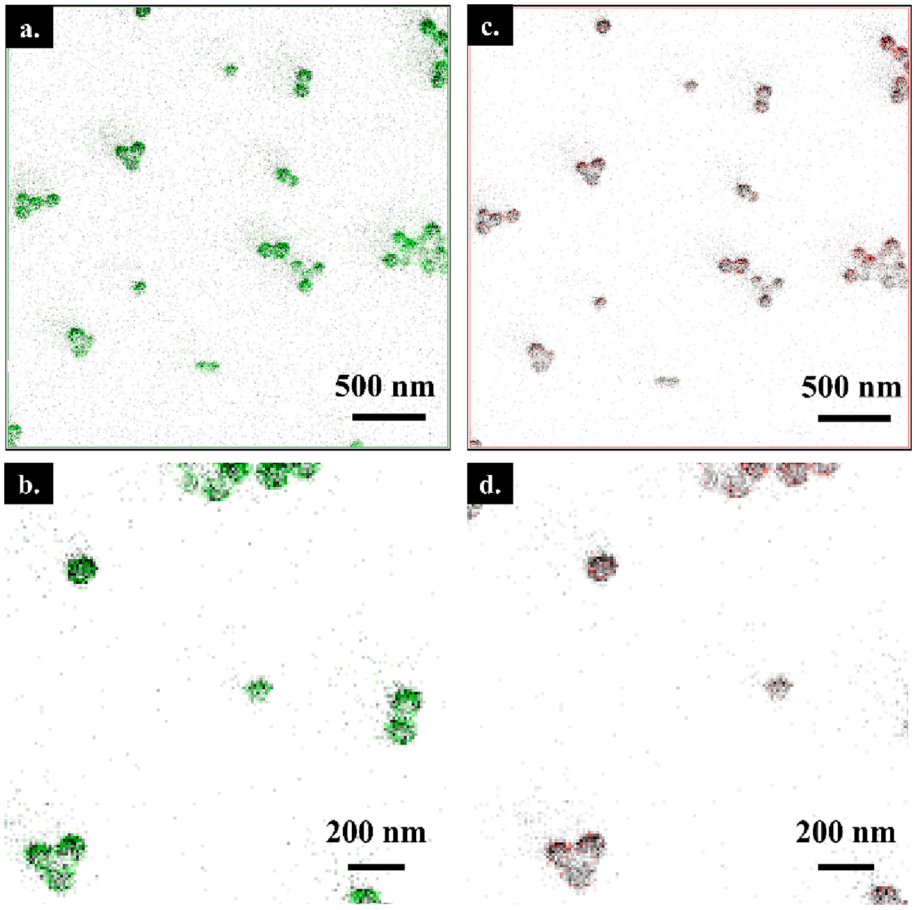

Fig. 3. HIM-SIMS elemental mapping of regio-selectively modified dendritic silica: oxygen (grey)/carbon (green) overlap (a, b), oxygen (grey)/bromine (red) overlap (c, d).

3.3. Characterization of silica-rubber composites and their mechanical properties

3.3.1. Effect of particle morphology and functionalization on rubber properties

The effect of silica fillers, and fillers in general, on a polymer matrix is a result of the four main ways the particles interact with the polymer chains, and how their dynamic is affected by these interactions [40–42]. The filler-filler interaction of silica is dependent on the hydrogen bonding of particles, which dictates how fillers interact, and is responsible for the aggregation of the particles. These interactions may be classified in two types. First, the low strain reversible interaction is responsible for reinforcement. It is assessed by the measurement of the drop of storage modulus at low strain, i.e. the Payne effect. This can be directly correlated to the rolling resistance and wet grip properties of a rubber compound [43]. Second, the high strain irreversible interaction is characterized by the Mullins effect, when a compound is deformed beyond a previous maximum. This effect can also include phenomenon such as filler-polymer debonding or crack initiation and propagation [44]. Moreover, fillers and polymer can interact in two ways, being first the steric hindrance of the particles over the polymer chain, resulting from the network of fillers trapping rubber, and from the covalent bonding of fillers with polymer when a coupling agent like mercapto organosilanes is used. Both are responsible for the reinforcement of the material. In a rubber compound, all these interactions work together and ultimately drive the mechanical properties of polymer-based nanocomposites. Consequently, the filler size and specific surface area, loading level, and surface modification are key parameters that will affect how and how much fillers interact with themselves and with the polymer chains. Fractal precipitated silicas like HDS 200MP are a gold standard and are commonly used in tire tread compounds. It consists in 10 nm primary particles in the form of large agglomerates (200 μm) **(see Figure S4 of Supporting Information)** that form a percolating network made of fractal shaped aggregates of medium size (50–100 nm) once mixed in the rubber (see **Figure S4 c and d**). This kind of silica is silanized in-situ by the addition of liquid organosilanes during the rubber mixing process. This filler reveals high interaction with the polymer thanks to the interaction with the trapped rubber within the fractal structure and its silanized surface. One limitation of such a filler architecture is the susceptibility to dislocations and breaks under mechanical stress, which increases hysteresis and impairs its reinforcing properties. It is important to note that the rubber recipe used in the present work is optimized for this kind of filler.

To identify the potential benefit of regio-selectively modified dendritic silica fillers, the effect of the filler morphology and its chemical modification were first investigated. Non-functionalized Stöber and stellate silica were used to show the impact of the porous structure and functionalization on the dispersion of fillers and on the mechanical properties of composites. Fig. 4 below presents the results of tensile test at break, the reinforcing index, and cyclic tensile test performed at 70 % of each sample maximum elongation. The reinforcing index is calculated as the ratio of the modulus at 150 % strain divided by the modulus at 50 % strain.

The non-porous and non-modified Stöber silica composites show the overall worst properties, with no strain hardening in tensile testing, low moduli and reinforcing index of 2.13, as well as the lowest stress at break of about 4 MPa. This composite is the only one unable to withstand>5 tensile cycles upon breaking. Non-modified stellate silica also displays no strain hardening and has an even lower reinforcing index of 1.77 despite its higher stress at break. This compound is capable of very high elongation, almost 800 % strain, and thus reach higher ultimate stress than Stöber particles. Interestingly, at low strain (below 25 %), the non-modified stellate particles provide the composite with a high strength (see Fig. 4**a.**), with a steeper increase of the strength compared to other samples. The porous structure seems to give an advantage over the non-porous Stöber particles in terms of ultimate properties and fatigue

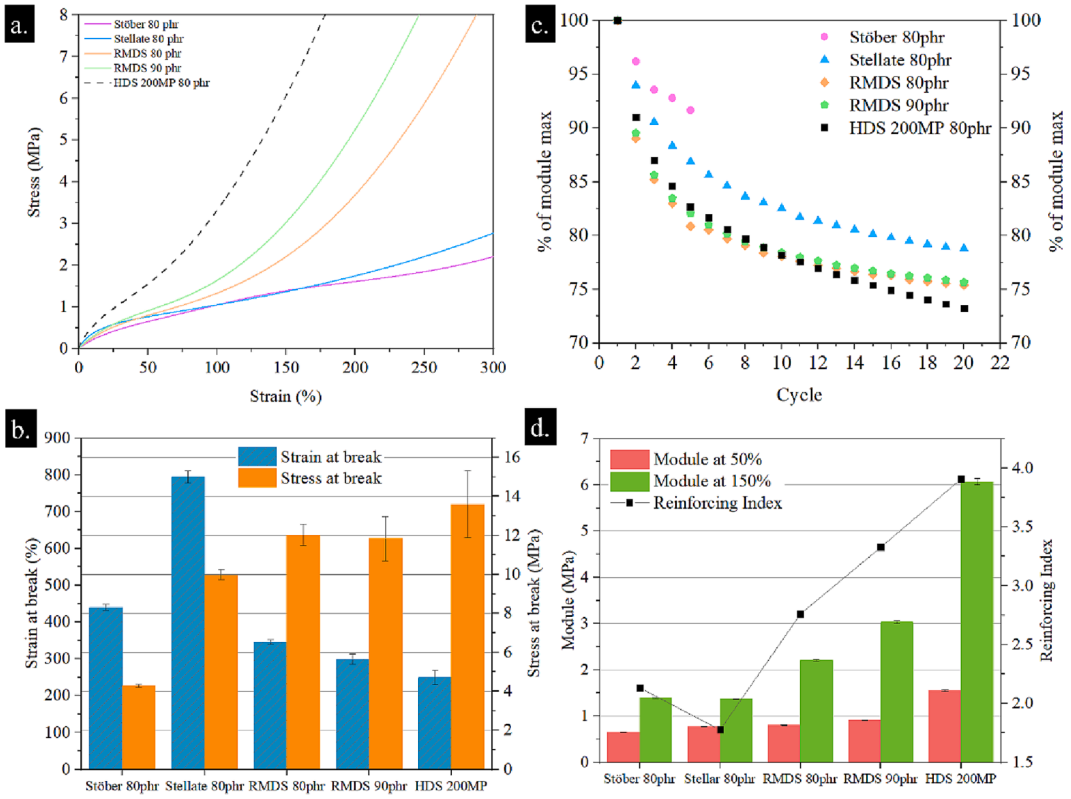

Fig. 4. Stress/Strain curves (a), evolution of maximum strength under cyclic tensile test (b), ultimate stress and strain at break (c) and reinforcing index (d) of composites materials.

resistance, as Stellate silica compounds show the lowest loss of strength over tensile cyclic testing. Without any coupling agent, silica-rubber phases are not efficiently crosslinked. In the case of Stöber or non-modified Stellate silica, only a linear deformation is observed after the initial deformation below 75 % strain. It can be suggested that the low-strain reinforcing effect of non-modified stellate silica arises from the hydrogen bonding of the bare silica surface. As RMDS contains about 9.5 % of silane (as reported in Fig. S1**c**.), the amount of silica for a given mass of filler is lower than for other pure silica fillers, especially HDS 200MP. To compensate this, 90 phr samples of pure RMDS on one side, and HDS 200MP on the other side, were tested. Results in Fig. S10**a** show that the tensile behavior of HDS 200MP silica-rubber samples is slightly worsen from 80 to 90 phr. The 90 phr HDS 200MP composite behaves similarly to the 70 phr sample. Graph b. of **Figure S10**, shows that the ultimate tensile properties are marginally improved by the addition of 10 phr from 80 to 90 phr. Based on these results, we concluded that the addition of 10 phr of HDS 200MP above 80 phr is marginally beneficial when the mechanical properties of the composite are considered. Indeed, the material reaches the percolation threshold at around 80 phr of HDS 200MP silica. STEM images in **Figure S11** support the conclusion that 80 phr is the optimal loading level for HDS 200MP, as the dispersion state is slightly worse at 90 phr. This leads to select HDS 200MP 80 phr as our reference sample. Unlike the two previous particles, RMDS silica shows strain hardening and has a higher reinforcing index of 2.76 and 3.32 at 80 phr and 90 phr respectively, as well as good ultimate properties, with ultimate strength of 12 and 11.8 MPa, respectively. The porous structure and regio-selective modification of the dendritic silica do provide obvious benefits over non-porous and non-modified porous silica. Though the additional 10 phr increases the reinforcement of the polymer, it does not compensate the mechanical properties discrepancy observed with the HDS 200MP fractal filler system. Dynamic Mechanical Analysis (DMA) was performed to further investigate the filler-filler interaction and understand the difference of behavior of RMDS particles versus the fractal HDS 200MP filler system. Results are presented in Fig. 5 below. The corresponding storage modulus E' at 30 °C measured by DMA are displayed in **Figure S6 of Supporting Information**.

The amplitude of the tan δ peak is reflecting the chain mobility of a polymer reaching a maximum at the glass transition T_g. In the case of filled polymers where the chain dynamic is restricted close to the filler particles, the tan δ peak amplitude is lowered as the polymer chain mobility is reduced. In the case of Stöber silica composites, the limited dispersion and absence of functionalization prevent significant interaction between fillers and polymer chains, resulting in high tan δ peak, similar to unfilled SBR. [45] Tan δ also characterizes the tendency of rubber to lose energy at a given mechanical solicitation frequency. According to the Williams-Landel-Ferry [46] relationship of the time–temperature equivalence, high temperatures are equivalent to low frequency and low temperature to high frequency. In the present case tan δ at 0 °C serves as the indicators of traction performances, and at 60 °C, it represents the rolling resistance of the composites [47,48]. Ideally, high energy losses are desired for traction and breaking, and minimal losses are targeted to reduce rolling resistance. In the case of Stöber composite the filler-polymer interaction is so weak that aggregates are barely affected by the composite deformation which is corroborated by the height of the tan δ peak, translating the high mobility of the polymer chains. The low level of Payne effect is another element explaining the lack of reinforcement. Indeed, the amount and size of aggregates do not lead to a reinforcing percolating network. Fig. 5**d** shows the results obtained for the four different types of silica here described at 80 phr filling degree with corresponding fitting curves. The plot shows a more pronounced Payne effect for the sample HDS 200 MP followed respectively by Stellate 80 phr, RMDS 80 phr and Stöber 80 phr. The same trend is observed for the modulus at dynamic strain amplitudes smaller than 1 %. The decay for the different types of silica indicates that in the case of HDS 200 MP the fractal particles are more prone to form aggregates than the other silica fillers here studied. These aggregates are subject to strain-induced breakage that leads to a pronounced decay of E' in the dynamic strain range studied. An interesting

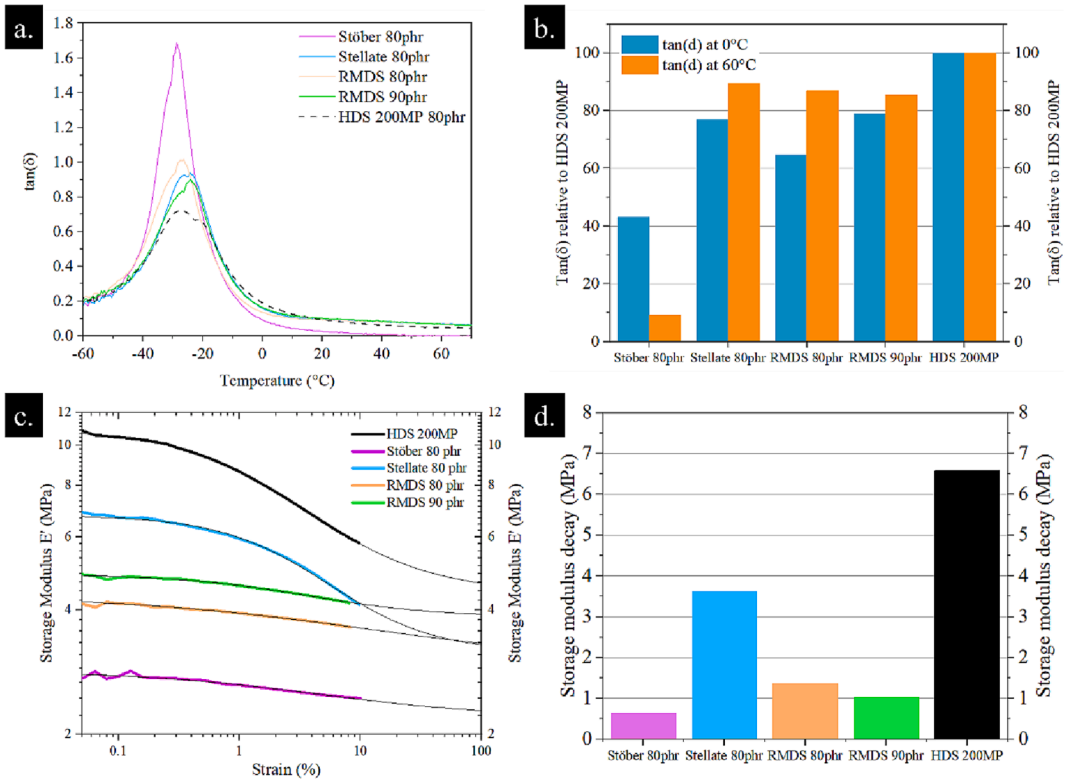

Fig. 5. Tan δ (at 1 Hz) curves of silica-rubber composites (a) and tan δ at 0 °C and 60 °C relative to HDS 200MP compound (b), Storage modulus E' vs Strain with corresponding Kraus fits (black lines) (c) and Payne effect storage modulus decay (d) (at 10 Hz).

comparison between Stellate 80 phr and RMDS 80 phr highlights how the different silanization affects the formation of aggregates as well. Stellate silica particles exhibit strong inter-particle interactions at low strain, most likely through hydrogen bonding, corroborating the tensile behavior of these composite. The fitting parameter $\Delta E'$ reported in **Table S3 of Supporting Information** shows that the Payne effect is more significant in the case of Stellate than for RMDS, indicating that in the case of the latter, the composite is less affected by a filler network breakage or fillers occur predominantly as single particles. On the other hand, the spherical Stöber particles lead to a low reinforcement as well as a weak decay of E'. As reported in **Table S3 of Supporting Information**, the values of m fitted for the samples under investigation are lower than the literature values and seem to be dependent on the type of filler. The discrepancy could be attributed to the shape of the fillers used in this work. While the Stöber particles are spherical, Stellate silica and RDMS are characterized by lower density with respect to HDS 200 MP. The different shape as well as the different distribution of the silane coupling agent at the surface of the particles could be responsible for the deviation from the expected fractal dimension of the clusters. In addition, from Fig. 5**d** it is evident that in the case of Stöber 80 phr and RDMS 80 phr, the decay of the storage modulus occurs close to the limit of the measured dynamic strain. For this reason, the fitted parameter m, closely related to the slope of the decaying function E' is subject to a high uncertainty. RMDS composites exhibit very low Payne effect, with an elastic modulus decay 1.36 MPa and 1.03 MPa for 80 phr and 90 phr composite respectively, when compared to non-modified Stellate or HDS 200MP (6.58 MPa decay). This features low filler-filler interactions in the composite. Consequently, the wet traction indicator tan δ at 0 °C of RMDS 80 phr is lower than Stellate or HDS 200MP. The 90 phr composite manages to slightly increase this parameter while maintaining low tan δ at 60 °C, but still this does not reach the level of HDS 200MP. The comparison of Stöber, non-modified stellate silica and RMDS indicates that the dendritic structure and its regio-selective modification bring more reinforcement to the polymer by crosslinking and trapping rubber in the porous structure. However, the filler-filler interactions are too weak to provide sufficient reinforcement and traction properties. Also, RMDS behaves as a low energy dispersion filler compared to HDS 200MP, as seen with the low tan δ at 0 °C and 60 °C values seen in Fig. 5**b**. It is beneficial in term of rolling resistance but not for the grip and traction. STEM images and computed tomography micrograph are shown in Fig. 6 and Fig. 7 respectively. Additional tomography numerical data of agglomerates and strain induced volume increase are presented in **Figure S7 and S8 of Supporting Information**.

Stöber and non-modified Stellate silica both display particles agglomeration. The presence of agglomerates diminishes the density of silica in the homogeneous areas and prevents to reach a reinforcing percolation network at which the polymer chains would be significantly affected by the particle density. This is supported by tomography in Fig. 7, where the severe agglomeration and lack of silanization of Stöber silica is responsible for debonding and cracks propagation, explaining the low mechanical properties. On the other side, despite the absence of silane, non-modified stellate silica shows a better dispersion but still some agglomeration. This might be due to higher mixing forces (**see Figure S5 of Supporting information**) employed for this compound, arising from hydrogen bonding of Stellate particles. The absence of silanization on stellate silica promotes the hydrogen bonding of particles and thus the reinforcement at low strain (below 25 %). At higher strain, filler-rubber interactions are nonexistent, resulting in the absence of strain hardening and a lower reinforcement. The slight reinforcement over Stöber particles is due to the higher surface area and formation of a filler network leading to higher interaction of the polymer with the porous structure. Finally, RMDS shows a great dispersive behavior with very little aggregates. The low-density area of the RMDS 80 phr sample seen in tomography (Fig. 7 **g.**) can be interpreted as spots where the concentration of particles is lower. This feature is also present in non-solicited rubber sample, indicating that it is an intrinsic feature of the compound itself and it is not caused by the mechanical deformation of the sample. The low volume fraction of stress-induced cavities translates the very good filler-rubber interaction within the composite. But no percolation network is formed, even at 90 phr. This may be due to the size and spherical nature of the RMDS particles, preventing an optimal contact and interlock of the particles. These observations lead to the conclusion that on its own, this filler system is unable to form a percolating network, unlike a fractal system like HDS 200MP.

Mechanical properties of composites and microscopy corroborate the model that a good reinforcing filler should display good filler-filler and filler-rubber interaction. The latter is obtained via the use of coupling and dispersive silanes that prevent silica aggregation, allow for a good dispersion and coupling with the polymer chains. The absence of silane in Stöber and non-modified stellate particles is clearly responsible for the low reinforcing properties, but results hint that the porous structure already bring reinforcement on its own. RMDS show very good properties for reinforcement and low energy dispersion, but the impossibility to form a percolating network prevent it to reach the level of fractal system in term of reinforcement or wet grip. To overcome this, we hypothesize that the use of HDS 200MP as an additive in small amount should increase the filler-polymer interaction by densifying the filler network and fill the gaps between the spherical RMDS particles.

3.3.2. *Dual-filler systems characterization and properties*

STEM images of composites and computed micro-tomography results are displayed in Fig. 8. The addition 10 phr of HDS 200MP clearly

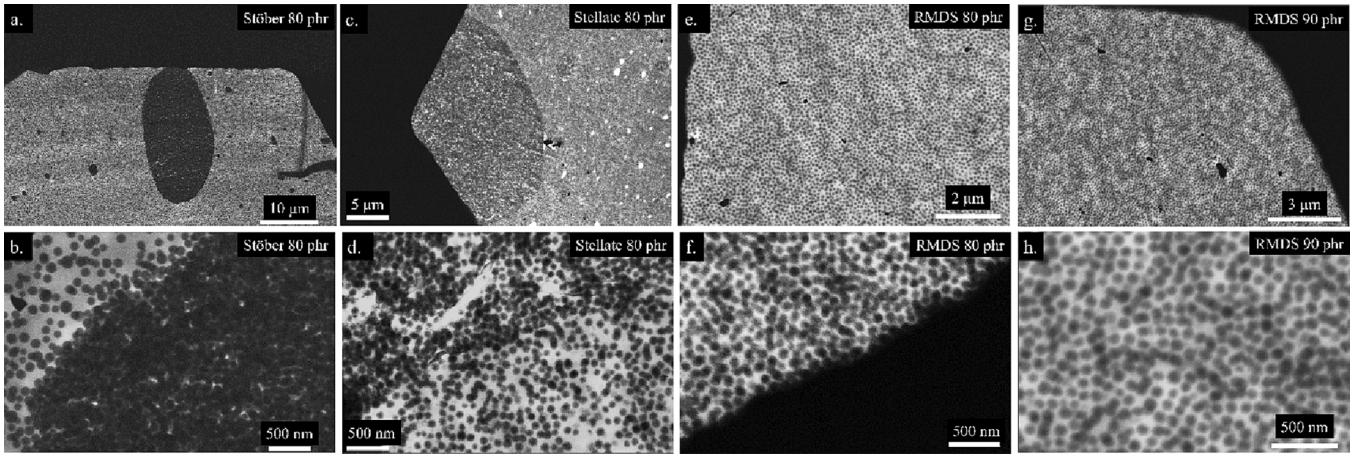

Fig. 6. STEM images of Stöber (a,b), non-modified Stellate (c,d), and RMDS silica-rubber at 80 phr (e,f) and 90 phr (g,h) composites in bright field mode.

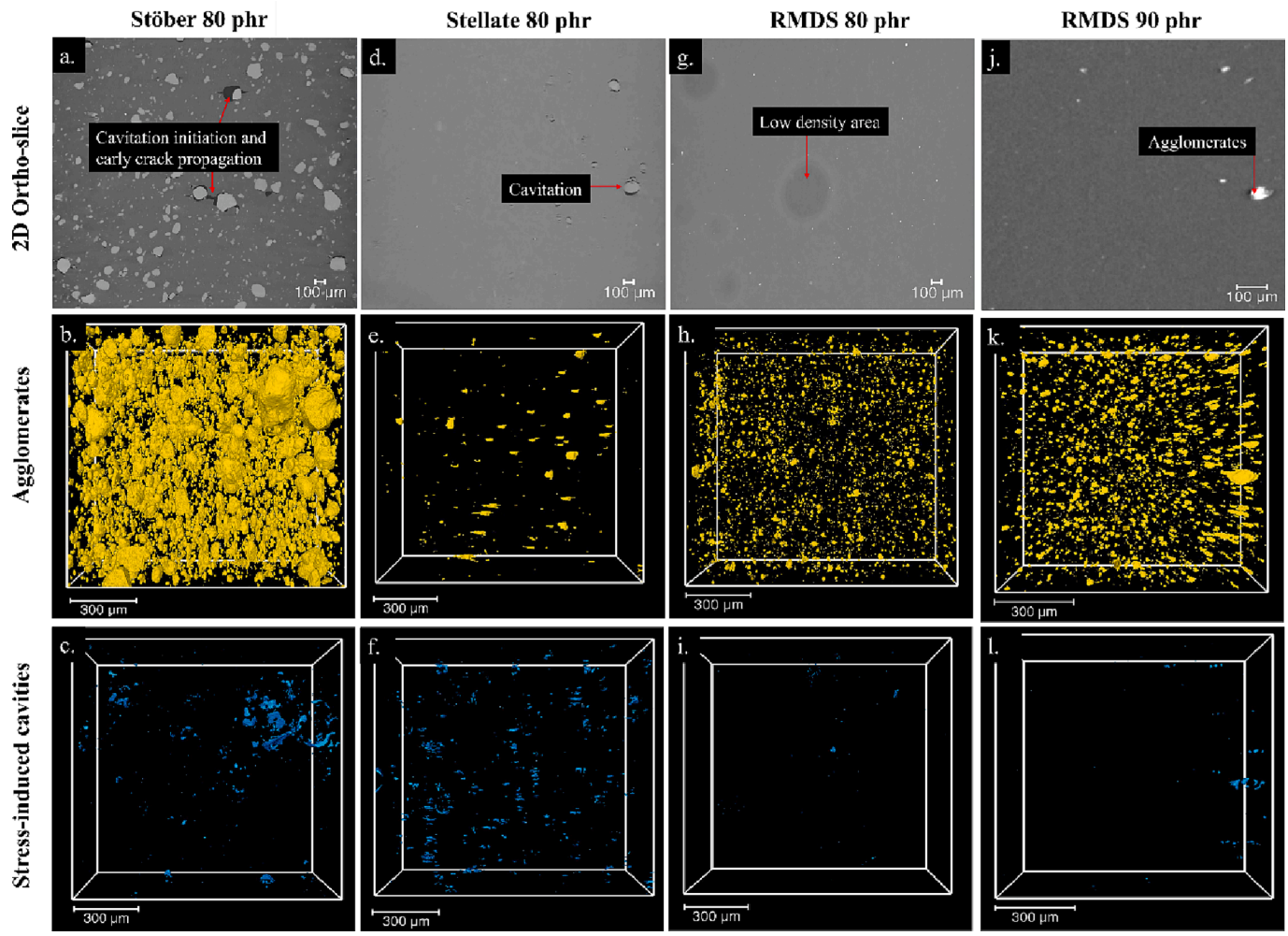

Fig. 7. 2D *ortho*-slice, agglomerates volume fraction (>5 µm) and strain-induced cavities (>5 µm) of Stöber (a,b,c), non-modified Stellate (d,e,f), RMDS 80 phr (g,h, i), and RMDS 90 phr (j,k,l) silica-rubber composites after cyclic tensile strength testing.

increases the particle density, and small HDS 200MP particles can be spotted in between the larger RMDS spheres. Additionally, low-density area previously seen in Fig. 7 are absent. Despite the increase in silica loading, RMDS shows no major agglomeration.

The composite shows minor agglomerates and almost no strain induced cavities. Interestingly, RMDS shows less agglomerates at 90 + 10 phr than 90 phr. This is likely because a higher filler loading induces higher mixing torque during compounding, as it can be seen in **Figure S5 of Supporting Information**. The resulting mechanical properties of dual filler composites are shown in Fig. 9 below. STEM images of composites at 80 + 5, 80 + 10 and 90 + 5 phr are available in of **Figure S9 of Supporting Information**.

The addition of HDS 200MP increases the reinforcement of the composites up to a point where RMDS 90 + 10 phr is higher than the pure fractal filler composite, with a reinforcing index of 4.15 versus 3.9 for HDS 200MP (Fig. 9**a**). RMDS 90 + 10 phr also display better fatigue properties as shown by the cyclic tensile results. The trade-off is a lower ultimate strain and consequently a lower stress at break for all composites over 90 phr of RMDS compared to 80 phr. But the main effect of this dual-filler system is the drastic increase of filler-polymer interaction, as shown by DMA data in Fig. 10.

The combination of the regio-selectively modified dendritic silica and the smaller fractal HDS 200MP allows to drastically increase the filler-filler interaction, as seen in the increase in storage modulus decay in Fig. 10**d**. The particle density also affects the filler-polymer network and limits the polymer chain mobility as seen in Fig. 10**a**. The increased level of interaction between filler and rubber is supported by the decrease of the tan δ peak intensity when increasing the filler loading. The addition of small amount of HDS 200MP increases the Payne effect linearly for 80 phr compounds, but the effect is more pronounced when 5 phr are added to 90 phr of RMDS. At the filler loading of about 90 + 5 phr, the percolation of the filler network is reached, and mechanical properties change drastically. This is seen especially for wet grip and rolling resistance indicator tan δ in Fig. 10**b**. The combination with HDS 200MP allows to improve the traction indicator tan δ at 0 °C for all samples, with the 90 + 10 phr combination surpassing the HDS 200MP while still having a lower rolling resistance. Interestingly, both tensile strength testing and DMA show that this filler combination seems to have a synergetic effect. The fact that the 90 phr HDS 200MP composite does not bring any additional reinforcement compared to 80 phr, as shown in **Figure S10 and S11**, enables us to confirm that it is not the additional 10 phr of fillers that brings more reinforcement, but the use of both fillers simultaneously at this specific loading. Overall, the 90 + 10 phr dual-filler sample benefits from the advantages of the two fillers: good fatigue resistance and lower rolling resistance due to RMDS silica, high wet grip indicator due to HDS 200MP (superior to the pure fractal filler sample), and good reinforcement due to both fillers.

The porous morphology of RMDS silica mimics a fractal structure and enable high interaction between silica particles and polymer chains while leading to a homogenous dispersion of particles with minimal agglomeration and strain induced cavities. RMDS can be qualified of an “unbreakable aggregate”. The addition of a small amount of HDS 200MP

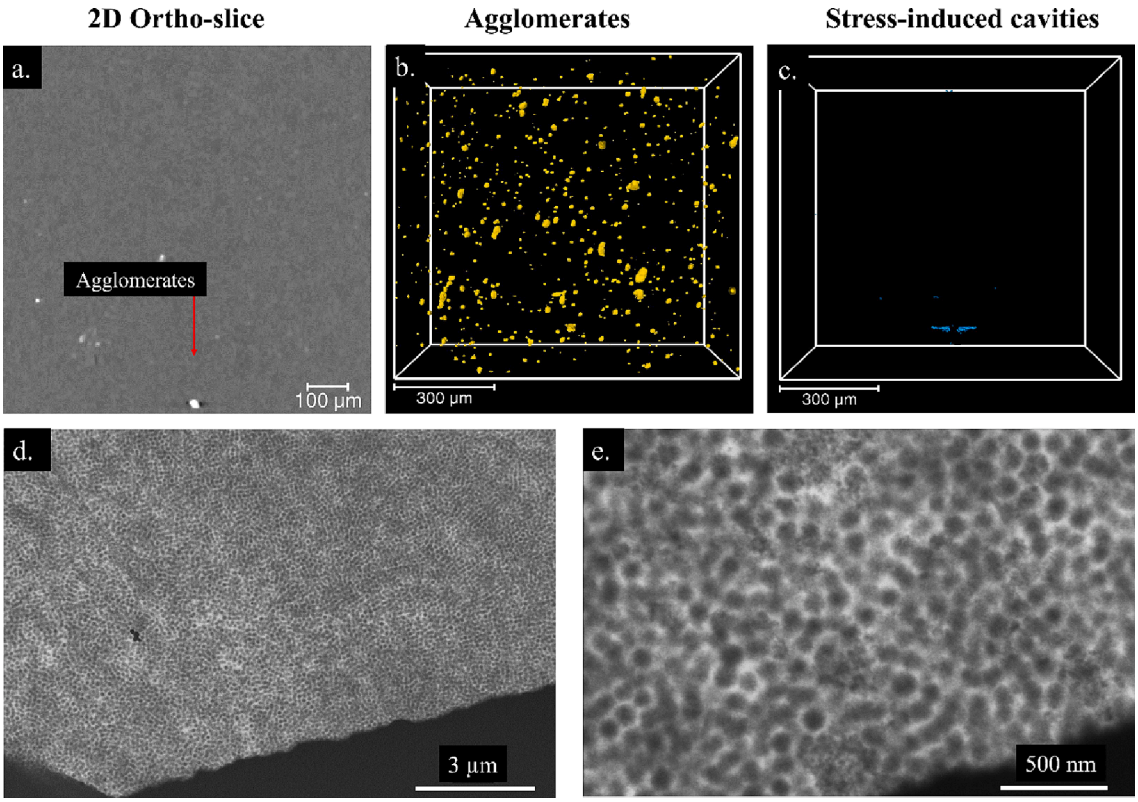

Fig. 8. 2D *ortho*-slice, agglomerates volume fraction (>5µm) and strain-induced cavities (>5µm) of RMDS 90 + 10 phr (a,b,c) and STEM images (d,e).

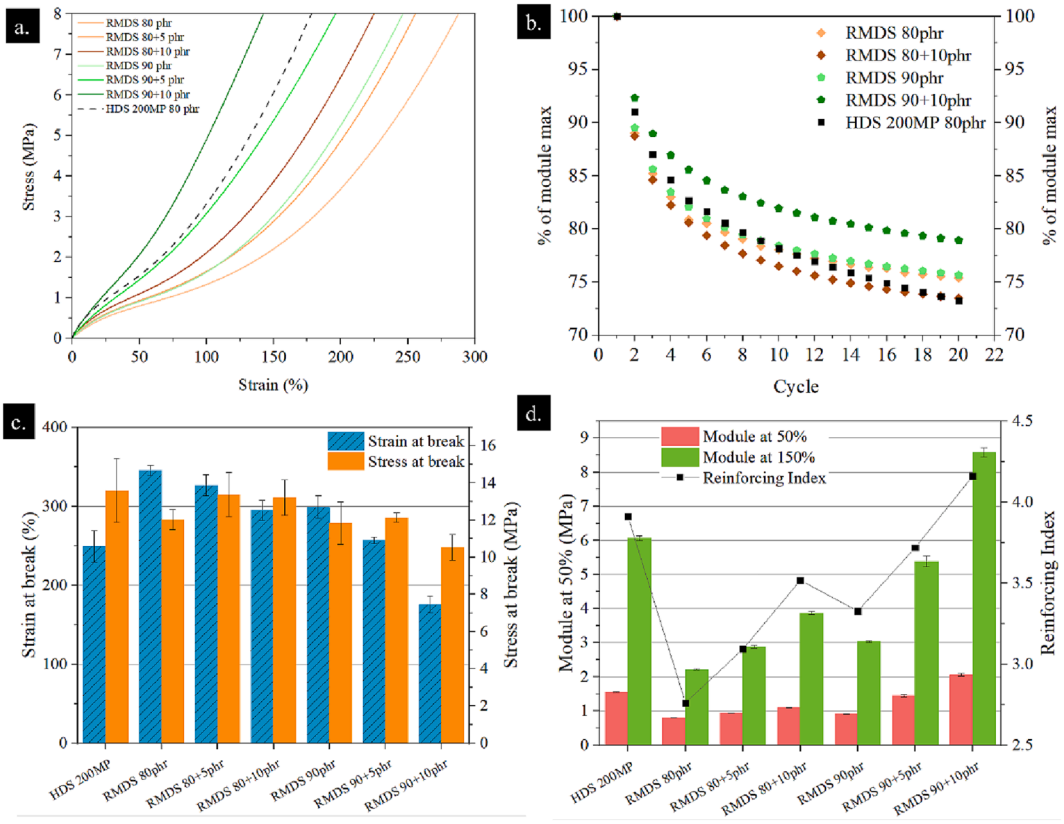

Fig. 9. Stress/Strain curves (a), evolution of maximum strength under cyclic tensile test (b), ultimate stress and strain at break (c) and reinforcing index (d) of dual-filler composites materials.

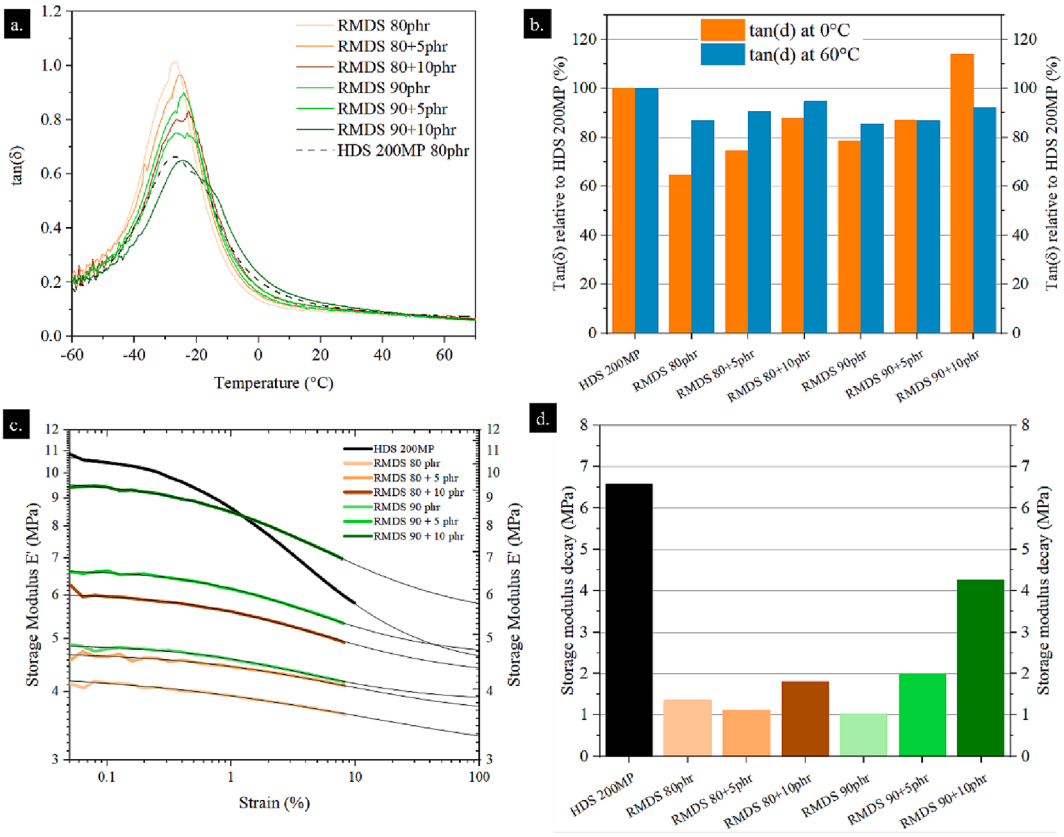

Fig. 10. Tan(δ) curves of silica-rubber composites (a) and tan δ at 0 °C and 60 °C relative to HDS 200MP compound (b), Storage modulus E' vs Strain with corresponding Kraus fits (black lines) (c) and Payne effect storage modulus decay (d).

fills the gaps between RMDS particles in the rubber matrix and enables to compensate for their lack of filler-filler interaction, as supported by the increase in Payne effect seen in Fig. 10**d**.

Under mechanical deformation and sufficient strain, silica particles are pulled apart one from another as the composite material is elongated. When large smooth particles without any silanization are used, silica particles do not interact with the polymer chains and barely restrain their dynamic, as in the case of the Stöber silica composite used in this study. For HDS 200MP, particle aggregates manage to trap rubber in so-called inter-particles porosity. In the case of RMDS, the intra-particle porosity plays the same role, but unlike HDS 200MP aggregates, RMDS particles cannot be pulled apart and do not suffer from permanent dislocation. Subsequently, RMDS composite behave much better under fatigue and show less hysteresis and Payne effect. Finally, the addition of a small amount of the HDS 200MP to RMDS composites enables to fill the gaps between the particles and further increases the filler-filler interaction without overly increasing the Payne effect, leading to a composite with superior reinforcement, wet grip and rolling resistance while keeping good fatigue resistance. This is a major breakthrough here as those three properties are usually antagonistic when their respective improvement is sought.

4. Conclusion

The use of porous silica particles as potent fillers for tire rubber has seen limited use for many years compared to nanometer-size fractal precipitated silica fillers. Indeed, the latter has shown to be more efficient in interacting with the polymer chains because of the fractal structure resulting from the mixing with the matrix. This percolating network enables high filler-polymer interactions by trapping rubber in interparticle porosity. High filler-filler interaction arises from the particle network, leading to good reinforcement. In this work are reported the synthesis and characterization of unique modified dendritic silica fillers with a regio-selective functionalization that are proven to be very efficient at reinforcing tire rubber with 110 nm spherical particles. The combination of the porous structure and the intricate silanization of particles allows the rubber to permeate into the pore and to crosslink with fillers while still allowing a great dispersion of particles. Microscopy, tomography, and mechanical properties characterization results presented here confirm the potential of such a filler technology. RMDS composites show minimal aggregation, cracks, and stress induced cavitation. The combination of RMDS with small amount of a smaller fractal silica filler increases the filler-filler interactions and enables better reinforcement than each filler on its own. Higher tensile strength and moduli, as well as better wet traction and rolling resistance properties are observed. Beyond the homogeneous distribution of particles in the rubber matrix, greater fatigue resistance properties of RMDS filler come from its capacity to behave as a high-interacting reinforcing aggregate regarding the polymer, but without suffering from the irreversible dislocation of those aggregates. It results in a better retention of the reinforcing properties over repeated deformation. The application of such a filler system for tire rubber reinforcement opens new perspectives in the engineering of tires with low rolling resistance and competitive traction with durable performances.

Funding Sources

The authors would like to thank the National Research Found of Luxembourg (FNR) for their financial support through the IPBG16/11514551/TireMat-Tech project.

Declaration of Competing Interest

The authors declare that they have no known competing financial

interests or personal relationships that could have appeared to influence the work reported in this paper.

Data availability

Data will be made available on request.

Acknowledgements

We thank Régis Vaudémont and Benoît Marcolini for their precious help on thermal characterization on our fillers and composite, Reiner Dieden and Chuanyu Yan for their help on NMR data processing, Stephan Westermann for is precious advice on dynamic mechanical rubber properties, and Jaafar Ghanbaja for his expertise in electron microscopy and elemental analysis. Finally, we thank Frédéric Addiego for his precious help on X-ray Tomography.

Appendix A. Supplementary data

Supplementary data to this article can be found online at https://doi.org/10.1016/j.cej.2023.141964.

References

[1] M. Staropoli, V. Rogé, E. Moretto, J. Didierjean, M. Michel, B. Duez, P. Steiner, G. Thielen, D. Lenoble, J.-S. Thomann, Hybrid silica-based fillers in nanocomposites: Influence of isotropic/isotropic and isotropic/anisotropic fillers on mechanical properties of styrene-butadiene (SBR)-based rubber, Polymers 13 (2021) 2413.

[2] Y. Lin, S. Liu, J. Peng, L. Liu, The filler–rubber interface and reinforcement in styrene butadiene rubber composites with graphene/silica hybrids: A quantitative correlation with the constrained region, Compos. A Appl. Sci. Manuf. 86 (2016) 19–30.

[3] R. Scotti, L. Conzatti, M. D'Arienzo, B. Di Credico, L. Giannini, T. Hanel, P. Stagnaro, A. Susanna, L. Tadiello, F. Morazzoni, Shape controlled spherical (0D) and rod-like (1D) silica nanoparticles in silica/styrene butadiene rubber nanocomposites: Role of the particle morphology on the filler reinforcing effect, Polymer 55 (2014) 1497–1506.

[4] L. Tadiello, M. D'Arienzo, B. Di Credico, T. Hanel, L. Matejka, M. Mauri, F. Morazzoni, R. Simonutti, M. Spirkova, R. Scotti, The filler–rubber interface in styrene butadiene nanocomposites with anisotropic silica particles: morphology and dynamic properties, Soft Matter 11 (2015) 4022–4033.

[5] Chiola, V., Ritsko, E.J. and Vanderpool, D.C. (1971) Process for Producing Low-Bulk Density Silica. Application No. US 3556725D, Publication No. US 3556725.

[6] J.S. Beck, J.C. Vartuli, W.J. Roth, M.E. Leonowicz, C. Kresge, K. Schmitt, C. Chu, D. H. Olson, E. Sheppard, S. McCullen, A new family of mesoporous molecular sieves prepared with liquid crystal templates, J. Am. Chem. Soc. 114 (1992) 10834–10843.

[7] D. Zhao, J. Feng, Q. Huo, N. Melosh, G.H. Fredrickson, B.F. Chmelka, G.D. Stucky, Triblock copolymer syntheses of mesoporous silica with periodic 50 to 300 angstrom pores, Science 279 (1998) 548–552.

[8] L. Palanikumar, E.S. Choi, J.Y. Cheon, S.H. Joo, J.H. Ryu, Noncovalent polymer-gatekeeper in mesoporous silica nanoparticles as a targeted drug delivery platform, Adv. Funct. Mater. 25 (2015) 957–965.

[9] F. Hou, Z. Teng, J. Ru, H. Liu, J. Li, Y. Zhang, S. Sun, H. Guo, Flower-like mesoporous silica nanoparticles as an antigen delivery platform to promote systemic immune response, Nanomed. Nanotechnol. Biol. Med. 42 (2022), 102541.

[10] F. Perton, S. Harlepp, G. Follain, K. Parkhomenko, J.G. Goetz, S. Bégin-Colin, D. Mertz, Wrapped stellate silica nanocomposites as biocompatible luminescent nanoplatforms assessed in vivo, J. Colloid Interface Sci. 542 (2019) 469–482.

[11] L.C. Lin, M. Thirumavalavan, J.F. Lee, Facile Synthesis of Thiol-functionalized Mesoporous Silica-Their Role for Heavy Metal Removal Efficiency. *CLEAN–Soil, Air*, Water 43 (2015) 775–785.

[12] B. Ghalei, A. Pournaghshband Isfahani, M. Sadeghi, E. Vakili, A. Jalili, Polyurethane-mesoporous silica gas separation membranes, Polym. Adv. Technol. 29 (2018) 874–883.

[13] A. Galarneau, J. Iapichella, D. Brunel, F. Fajula, Z. Bayram-Hahn, K. Unger, G. Puy, C. Demesmay, J.L. Rocca, Spherical ordered mesoporous silicas and silica monoliths as stationary phases for liquid chromatography, J. Sep. Sci. 29 (2006) 844–855.

[14] X. Yang, D. Chen, S. Liao, H. Song, Y. Li, Z. Fu, Y. Su, High-performance Pd–Au bimetallic catalyst with mesoporous silica nanoparticles as support and its catalysis of cinnamaldehyde hydrogenation, J. Catal. 291 (2012) 36–43.

[15] Y. Luo, J. Lin, Synthesis and characterization of Co (II) salen functionalized MCM-41-type hybrid mesoporous silicas and their applications in catalysis for styrene oxidation with H2O2, Microporous Mesoporous Mater. 86 (2005) 23–30.

[16] N. Suzuki, Y. Kamachi, K. Takai, S. Kiba, Y. Sakka, N. Miyamoto, Y. Yamauchi, Effective use of mesoporous silica filler: comparative study on thermal stability and transparency of silicone rubbers loaded with various kinds of silica particles, Eur. J. Inorg. Chem. 2014 (2014) 2773–2778.

[17] Y. Luo, J.P. Wang, X. Cui, Y. Fu, G.L. Li, W. Wang, Surface-modified mesoporous silica nanorods for the highly aging resistance rubber through controlled release of antioxidant, Polym. Adv. Technol. 32 (2021) 3384–3391.

[18] D. Zhao, S. Ge, E. Senses, P. Akcora, J. Jestin, S.K. Kumar, Role of filler shape and connectivity on the viscoelastic behavior in polymer nanocomposites, Macromolecules 48 (2015) 5433–5438.

[19] R. Yang, Y. Song, Q. Zheng, Payne effect of silica-filled styrene-butadiene rubber, Polymer 116 (2017) 304–313.

[20] J. Ramier, C. Gauthier, L. Chazeau, L. Stelandre, L. Guy, Payne effect in silica-filled styrene–butadiene rubber: influence of surface treatment, J Polym Sci B 45 (2007) 286–298.

[21] M. Staropoli, D. Gerstner, M. Sztucki, G. Vehres, B. Duez, S. Westermann, D. Lenoble, W. Pyckhout-Hintzen, Hierarchical scattering function for silica-filled rubbers under deformation: Effect of the initial cluster distribution, Macromolecules 52 (2019) 9735–9745.

[22] S. Nuntang, S. Poompradub, S. Butnark, T. Yokoi, T. Tatsumi, C. Ngamcharussrivichai, Novel mesoporous composites based on natural rubber and hexagonal mesoporous silica: synthesis and characterization, Mater. Chem. Phys. 143 (2014) 1199–1208.

[23] L.D. Perez, L. Sierra, B.L. Lopez, Effect of the filler characteristics on the miscibility of styrene-butadiene rubber and nitrile-butadiene rubber blends, Polym. Eng. Sci. 48 (2008) 1986–1993.

[24] L.D. Perez, B.L. Lopez, Thermal characterization of SBR/NBR blends reinforced with a mesoporous silica, J. Appl. Polym. Sci. 125 (2012) E327–E333.

[25] H. Acharya, S.K. Srivastava, Mechanical, thermo-mechanical, thermal, and swelling properties of EPDM-organically modified mesoporous silica nanocomposites, Polym. Compos. 38 (2017) E371–E380.

[26] Y. Kojima, T. Matsuoka, H. Takahashi, Preparation of nylon 66/mesoporous molecular sieve composite under high pressure, J. Appl. Polym. Sci. 74 (1999) 3254–3258.

[27] N. Wang, M. Li, J. Zhang, Polymer-filled porous MCM-41: An effective means to design polymer-based nanocomposite, Mater. Lett. 59 (2005) 2685–2688.

[28] S. Kiba, N. Suzuki, Y. Okawauchi, Y. Yamauchi, Prototype of low thermal expansion materials: fabrication of mesoporous silica/polymer composites with densely filled polymer inside mesopore space, Chemistry–An Asian Journal 5 (2010) 2100–2105.

[29] X. Ji, J.E. Hampsey, Q. Hu, J. He, Z. Yang, Y. Lu, Mesoporous silica-reinforced polymer nanocomposites, Chem. Mater. 15 (2003) 3656–3662.

[30] Z. Zhou, S. Zhu, D. Zhang, Grafting of thermo-responsive polymer inside mesoporous silica with large pore size using ATRP and investigation of its use in drug release, J. Mater. Chem. 17 (2007) 2428–2433.

[31] I. Park, Z. Wang, T.J. Pinnavaia, Assembly of large-pore silica mesophases with wormhole framework structures from α, ω-diamine porogens, Chem. Mater. 17 (2005) 383–386.

[32] I. Park, T.J. Pinnavaia, Mesocellular silica foam as an epoxy polymer reinforcing agent, Adv. Funct. Mater. 17 (2007) 2835–2841.

[33] J. Jiao, X. Sun, T.J. Pinnavaia, Reinforcement of a rubbery epoxy polymer by mesostructured silica and organosilica with wormhole framework structures, Adv. Funct. Mater. 18 (2008) 1067–1074.

[34] E. Moretto, J.o.P. Fernandes, M. Staropoli, V. Rogé, P. Steiner, B. Duez, D. Lenoble, J.-S. Thomann, Dual-Silane Premodified Silica Nanoparticles— Synthesis and Interplay between Chemical, Mechanical, and Curing Properties of Silica–Rubber Nanocomposites: Application to Tire Tread Compounds, ACS Omega 7 (21) (2022) 17692–17702.

[35] J. Kecht, A. Schlossbauer, T. Bein, Selective functionalization of the outer and inner surfaces in mesoporous silica nanoparticles, Chem. Mater. 20 (2008) 7207–7214.

[36] V. Cauda, A. Schlossbauer, J. Kecht, A. Zürner, T. Bein, Multiple core– shell functionalized colloidal mesoporous silica nanoparticles, J. Am. Chem. Soc. 131 (2009) 11361–11370.

[37] K. Zhang, L.-L. Xu, J.-G. Jiang, N. Calin, K.-F. Lam, S.-J. Zhang, H.-H. Wu, G.-D. Wu, B. Albela, l., Bonneviot, L., Facile large-scale synthesis of monodisperse mesoporous silica nanospheres with tunable pore structure, J. Am. Chem. Soc. 135 (2013) 2427–2430.

[38] K. Möller, J. Kobler, T. Bein, Colloidal suspensions of mercapto-functionalized nanosized mesoporous silica, J. Mater. Chem. 17 (2007) 624–631.

[39] N.T. Vo, A.K. Patra, D. Kim, Pore size and concentration effect of mesoporous silica nanoparticles on the coefficient of thermal expansion and optical transparency of poly (ether sulfone) films, PCCP 19 (2017) 1937–1944.

[40] P. Akcora, S.K. Kumar, J. Moll, S. Lewis, L.S. Schadler, Y. Li, B.C. Benicewicz, A. Sandy, S. Narayanan, J. Ilavsky, "Gel-like" mechanical reinforcement in polymer nanocomposite melts, Macromolecules 43 (2010) 1003–1010.

[41] C. Bartholome, E. Beyou, E. Bourgeat-Lami, P. Cassagnau, P. Chaumont, L. David, N. Zydowicz, Viscoelastic properties and morphological characterization of silica/polystyrene nanocomposites synthesized by nitroxide-mediated polymerization, Polymer 46 (2005) 9965–9973.

[42] J. Fröhlich, W. Niedermeier, H.-D. Luginsland, The effect of filler–filler and filler–elastomer interaction on rubber reinforcement, Compos. A Appl. Sci. Manuf. 36 (2005) 449–460.

[43] N. Vleugels, W. Pille-Wolf, W.K. Dierkes, J.W. Noordermeer, Understanding the influence of oligomeric resins on traction and rolling resistance of silica-reinforced tire treads, Rubber Chem. Technol. 88 (2015) 65–79.

[44] C. Federico, H. Padmanathan, O. Kotecký, R. Rommel, G. Rauchs, Y. Fleming, F. Addiego, Resolving cavitation in silica-filled styrene-butadiene rubber composites upon cyclic tensile testing, Polym. Test. 100 (2021), 107274.

[45] Z. Liu, H. Zhang, S. Song, Y. Zhang, Improving thermal conductivity of styrene-butadiene rubber composites by incorporating mesoporous silica@ solvothermal reduced graphene oxide hybrid nanosheets with low graphene content, Compos. Sci. Technol. 150 (2017) 174–180.
[46] M.L. Williams, R.F. Landel, J.D. Ferry, The temperature dependence of relaxation mechanisms in amorphous polymers and other glass-forming liquids, J. Am. Chem. Soc. 77 (1955) 3701–3707.
[47] H. Takino, R. Nakayama, Y. Yamada, S. Kohjiya, T. Matsuo, Viscoelastic properties of elastomers and tire wet skid resistance, Rubber Chem. Technol. 70 (1997) 584–594.
[48] Y. Li, B. Han, S. Wen, Y. Lu, H. Yang, L. Zhang, L. Liu, Effect of the temperature on surface modification of silica and properties of modified silica filled rubber composites, Compos. A Appl. Sci. Manuf. 62 (2014) 52–59.